J. Appl. Comput. Mech., 6(SI) (2020) 1270-1282
DOI: 10.22055/JACM.2020.32402.2008

ISSN: 2383-4536
jacm.scu.ac.ir

Shahid Chamran University of Ahvaz

Journal of Applied and Computational Mechanics

Research Paper

# Explicit and Implicit Finite -Volume Methods for Depth Averaged Free-Surface Flows

Evangelia D. Farsirotou[1], Alexander D. Panagiotopoulos[2], Johannes V. Soulis[3]

[1] Department of Icthyology and Aquatic Environment, University of Thessaly, Fytoko st. N. Ionia, Volos, 38446, Greece, Email: efars@uth.gr

[2] Department of Civil Engineering, Democrition University of Thrace, Fluid Mechanics/Hydraulic Division, Xanthi, 67100, Greece, Email: panagal@otenet.gr

[3] Department of Civil Engineering, Democrition University of Thrace, Fluid Mechanics/Hydraulic Division, Xanthi, 67100, Greece, Email: soulis@civil.duth.gr

Received January 27 2020; Revised March 27 2020; Accepted for publication March 30 2020.
Corresponding author: E.D. Farsirotou (efars@uth.gr)


**Abstract.** In recent years, much progress has been made in solving free-surface flow variation problems in order to prevent flood environmental problems in natural rivers. Computational results and convergence acceleration of two different (explicit and implicit numerical techniques) finite-volume based numerical algorithms, for depth-averaged subcritical and/or supercritical, free-surface, steady flows in channels, are presented. The implicit computational model is a bi-diagonal, finite-volume numerical scheme, based on MacCormack's predictor-corrector technique and uses the semi-linearization matrices for the governing Navier-Stokes equations which are expressed in terms of diagonalization. This implicit numerical scheme puts primary emphasis to solution convergence using non-orthogonal local coordinate system. The explicit formulation uses volume integrals to solve the governing flow equations. Computational results and convergence performance between the implicit and the explicit finite-volume numerical schemes, for incompressible, viscous, depth-averaged free-surface, steady flows are presented. Implicit and explicit computational results are satisfactorily compared with available measurements. The implicit bi-diagonal technique yields fast convergence compared to the explicit one at the expense of programming effort. Iterations require to achieve convergence solution error of less than $10^{-5}$, can be reduced down to 90.0 % in comparison to analogous flows with using explicit numerical technique.

**Keywords**: Explicit Integral Method, Implicit Bidiagonal Finite-Volume, Water Depth.

## 1. Introduction

Significant advances have been made in Computational Fluid Dynamics (CFD) applied to water surface variation in open channels. Nowadays, finite-difference, finite-element and finite-volume numerical techniques are available for two-dimensional, steady, viscous, free-surface flow calculations. However, most of these techniques are slow in their convergence. The implicit time-dependent techniques, which are not subject to the conventional stability condition of explicit methods, are the most computationally efficient techniques for tackling free-surface flows. Most of the implicit techniques require tri-diagonal or penta-diagonal system solution of equations resulting into considerable Central Processing Unit (CPU) time consumption. Implicit formulations that perform inversion of only upper or lower block bi-diagonal matrices are numerous. Initially, these techniques have been applied for compressible flow equations solution.

MacCormack [10] presented an implicit analog of his earlier widely used explicit method. Soulis [18] developed an explicit finite-volume technique for either subcritical or supercritical flows. Predictions agreed well with experimental measurements and/or other numerical method results. However, the convergence, particularly for subcritical flows, was relatively slow due to inherent CFL (Courant–Frieddrichs–Levy) time step restriction. For depth-averaged free-surface flows in complex channel geometries it is convenient to make predictions using a non-orthogonal boundary fitted computational mesh, Soulis [18]. A transformation was introduced through which quadrilaterals in the physical domain (global) were mapped into squares in the computational domain (local system). The greatest advantage of the above transformation was the accuracy and ease of application of the various types of solid and fluid boundary conditions which were required to be satisfied. Depth-averaged models have also been developed by Molls and Chaudhry [13], using a second order accurate Beam and Warming approximation for the time differencing and Bradford and Sanders [1], using a finite-volume method for unsteady, two-dimensional, shallow-water flow over arbitrary topography with moving lateral boundaries caused by flooding or recession. Farsirotou et al. [2] developed a fully coupled two-dimensional subcritical and/or supercritical, finite-volume numerical method to solve the non-linear, parabolic, partial differential governing equations in an integral form. The technique was applied to a series of finite-volumes with adjacent volumes sharing a common face, in a non-transformed grid, in order to calculate free-surface and bed variations in alluvial channels. Klonidis and Soulis [8] reported depth-averaged free-surface flow and Navier-Stokes equations solution with pseudo-compressibility technique for incompressible and viscous flow using second order implicit, finite-volume scheme capable of achieving fast convergence. Implicit bi-diagonal numerical scheme for 2D flood wave simulation was reported, Sun [12], using similar to Panagiotopoulos and Soulis [15] implicit technique approach. Moreover, Sheng et al. [17] presented a hydrodynamic model based on the two-dimensional shallow water equations and Godunov-type finite-volume scheme for simulating flood wave propagation. Fernandez et al. [3] presented an implicit method for solving the 2D shallow water equations based on the first order Roe's scheme, in the framework of finite volume methods. The computational fluid dynamic model FLUENT was used by Menni et al. [11] in order to simulate incompressible, steady, turbulent flow and heat transfer based on finite volume numerical technique, Gholami et al [6] used the same numerical model for the simulation of the complex flow pattern in bend open channels, Fu and Jin [4] investigated bed roughness effect on open channel flow and Naik at al [14] performed numerical analysis of hydrodynamic parameters variation in compound channels with the aforementioned model. Periyadurai at al [16] studied numerically natural convection flow using a finite volume numerical method and examined the effect of different parameters on the flow and heat transfer rate. Other numerical simulation studies can be found in literature as Vagheian and Talebi [20] and Gaffar et al [5] that evaluate computational results according to different conditions providing that it is important to develop an accurate and fast convergence numerical simulation methodology.

The goal of the current work is to investigate the convergence acceleration of an implicit bi-diagonal, finite-volume numerical scheme, Panagiotopoulos and Soulis [15], based on MacCormack's predictor- corrector technique compared to convergence history of an explicit finite-volume numerical method, Farsirotou [21] and Farsirotou et al [2]. Numerical results of free-surface flow variation were compared with available measurements elucidating the reliability of the applied numerical schemes. Applications refer to supercritical flows in the Rouse et al. [22] expansion channel, at various inflow conditions. Comparisons of the convergence performance between the implicit and the explicit finite-volume numerical schemes, for depth-averaged free-surface, steady flows was investigated providing the efficiency of the implicit method. The number of necessary computational iterations was significantly decreased applying the implicit technique.

## 2. Hydrodynamic Equations

The channel flow will be assumed to be homogeneous, incompressible, viscous, with hydrostatic pressure distribution and absence of Coriolis and wind forces. The governing two-dimensional free-surface flow equations for the physical domain, are described as Soulis [18] and Farsirotou et al. [2]:

$$\frac{\partial E}{\partial t}+\frac{\partial F}{\partial x}+\frac{\partial G}{\partial y}=Q \tag{1a}$$

The variables E, F, G, and Q are defined in matrix forms as follows:

$$E=\begin{bmatrix} h \\ hu \\ hv \end{bmatrix},\quad F=\begin{bmatrix} hu \\ hu^2+gh^2/2 \\ huv \end{bmatrix},\quad G=\begin{bmatrix} hv \\ huv \\ hv^2+gh^2/2 \end{bmatrix},\quad Q=\begin{bmatrix} 0 \\ -gh\left(S_{ox}-S_{fx}\right) \\ -gh\left(S_{oy}-S_{fy}\right) \end{bmatrix} \tag{1b}$$

The first line of the matrices refers to the continuity equation while the second and third lines refer to the x-momentum and y-momentum equations, respectively. Here x and y represent the Cartesian co-ordinate positions in the longitudinal and transverse directions respectively, t is the time, u and v are the average velocity components in the x and y directions, h is the water depth and g is the gravity acceleration, The bottom slopes $S_{ox}$ and $S_{oy}$ in x and y directions, respectively, are defined as $S_{ox}=-\partial z/\partial x$ and $S_{oy}=-\partial z/\partial y$ where z represents the bottom elevation. Flow friction slopes $S_{fx}$ and $S_{fy}$ are defined as Kassem and Chaudhry [7]:

$$S_{fx}=\frac{n^2u\sqrt{\left(u^2+v^2\right)}}{h^{4/3}}\quad,\qquad S_{fy}=\frac{n^2v\sqrt{\left(u^2+v^2\right)}}{h^{4/3}} \tag{2}$$

*n* is the Manning's flow friction coefficient. By writing the equation for frictional resistance in this way, it was assumed that all flow resistance is due to bottom friction, thus neglecting the boundary layers on the side walls. The stresses due to depth averaging are difficult to quantify and are customarily neglected (Molls, et al. [12]). The time derivative terms in the flow equations are simply a convenient way to iterate to a steady-state solution. The flow solution is closed with appropriate boundary conditions. Subcritical and supercritical flows are considered. For subcritical flow entrance, at the upstream end, two flow conditions are needed while at the downstream end one flow condition must be specified. For supercritical flow entrance all three flow conditions must be specified at the upstream end.

## 3. Implicit Finite-Volume Numerical Method

### 3.1 Transformation of Flow Equations

In the present numerical scheme quadrilaterals in the physical (global) domain will be separately mapped into squares in the computational (local) domain by independent transformations from Cartesian x, y to local ξ, η coordinates, as shown in Fig.1. Moreover, a schematic configuration of the implicit finite-volume numerical method is presented. The quadrilaterals are packed around the boundaries of the hydraulic structure and cover the whole flow field. The computational mesh, thus formed is comprised of equidistantly located computational nodes. An advantage of the applied transformation is the accuracy and the ease of application of the various types of boundary conditions. Variable density computational grids can also be applied in order to properly model the flow field.

Let $\left[J^{-1}\right]$ be the transformation matrix from the physical to computational local coordinate system as:

$$J=\frac{1}{x_\xi y_\eta-x_\eta y_\xi}=\xi_x\eta_y-\xi_y\eta_x \tag{3}$$

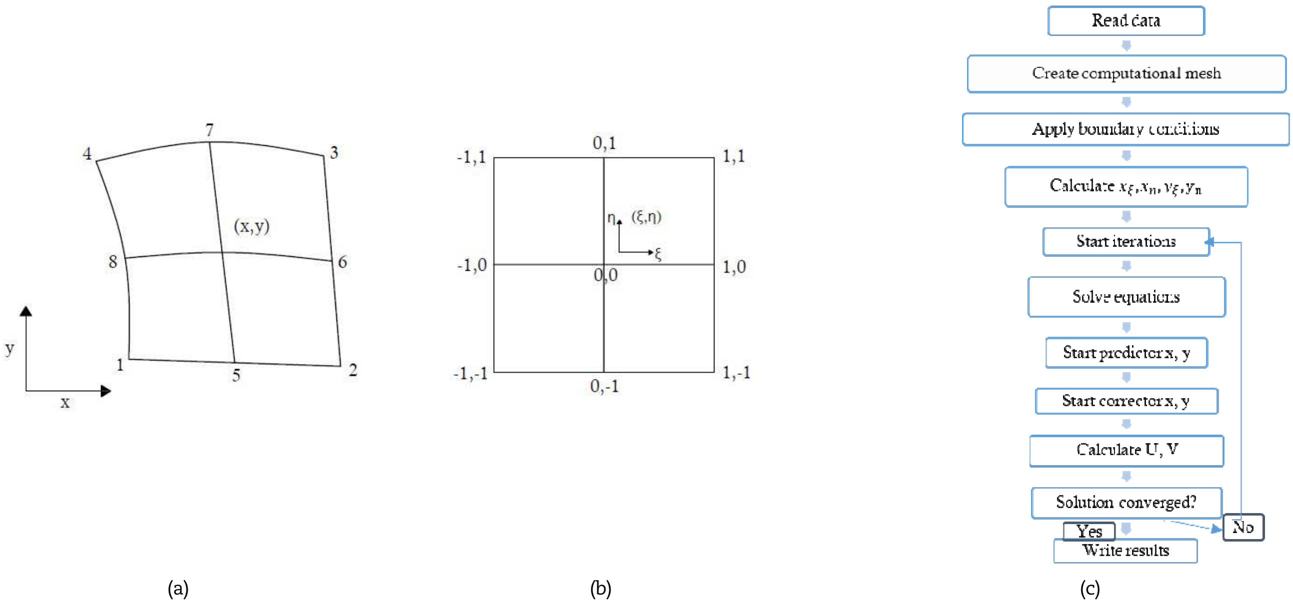


**Fig. 1.** Transformed grid from physical to local coordinates, a) physical domain, b) computational domain and c) schematic configuration of the implicit method.

The following relations hold:

$$\frac{\partial \xi}{\partial x} = J\,\frac{\partial y}{\partial \eta}\,,\quad \frac{\partial \xi}{\partial y} = -J\,\frac{\partial x}{\partial \eta}\,,\quad \frac{\partial \eta}{\partial x} = -J\,\frac{\partial y}{\partial \xi}\,,\quad \frac{\partial \eta}{\partial y} = J\,\frac{\partial x}{\partial \xi} \tag{4}$$

Equation (1) is transformed into the local coordinate system $\xi,\eta$ as:

$$\frac{\partial \hat{E}}{\partial t} + \frac{\partial \hat{F}}{\partial \xi} + \frac{\partial \hat{G}}{\partial \eta} = \hat{Q} \tag{5}$$

In which $\hat{E} = E / J$ , $\hat{F} = \left(F\xi_x + G\xi_y\right) / J$ , $\hat{G} = \left(F\eta_x + G\eta_y\right) / J$ and $\hat{Q} = Q/J$ . The velocity components u, v in the physical domain are related to the U, V velocity components in the computational domain with the following equations:

$$U = \frac{\partial \xi}{\partial x}u + \frac{\partial \xi}{\partial y}v\,,\qquad V = \frac{\partial \eta}{\partial x}u + \frac{\partial \eta}{\partial y}v \tag{6}$$

### 3.2 Implicit Numerical Scheme

The method of numerical integration of eq. (5) has been adopted from MacCormack [10]. The scheme is an implicit finite-volume method for time-integrating of the Navier-Stokes equations. It is a second order accurate in space and time scheme, unconditionally stable and very efficient in that no block or scalar tridiagonal inversions are required to be calculated. Equation (5) is integrated by the following implicit predictor-corrector set of finite-difference equations:

Predictor:

$$\begin{gathered}
\text{step1:}\quad \Delta\hat{E}^{n}_{i,j} = -\Delta t\left(\frac{\Delta^{+}\hat{F}^{\,n}_{i,j}}{\Delta\xi} + \frac{\Delta^{+}\hat{G}^{\,n}_{i,j}}{\Delta n} - \hat{Q}^{n}\right) \\
\text{step2:}\quad \left(I - \Delta t\,\frac{\Delta^{+}\left|\hat{A}\right|^{n}}{\Delta\xi}\right)\left(I - \Delta t\,\frac{\Delta^{+}\left|\hat{B}\right|^{n}}{\Delta n}\right)\delta\hat{E}^{\overline{n+1}}_{i,j} = \Delta\hat{E}^{n}_{i,j} \\
\text{step 3:}\quad \hat{E}^{\overline{n+1}}_{i,j} = \hat{E}^{n}_{i,j} + \delta\hat{E}^{\overline{n+1}}_{i,j}
\end{gathered} \tag{7}$$

Corrector:

$$\begin{gathered}
\text{step 4:}\quad \Delta\hat{E}^{\overline{n+1}}_{i,j} = -\Delta t\left(\frac{\Delta^{-}\hat{F}^{\,\overline{n+1}}_{i,j}}{\Delta\xi} + \frac{\Delta^{-}\hat{G}^{\,\overline{n+1}}_{i,j}}{\Delta n} - \hat{Q}^{\overline{n+1}}\right) \\
\text{step 5:}\quad \left(I + \Delta t\,\frac{\Delta^{-}\left|\hat{A}\right|^{\overline{n+1}}}{\Delta\xi}\right)\left(I + \Delta t\,\frac{\Delta^{-}\left|\hat{B}\right|^{\overline{n+1}}}{\Delta n}\right)\delta\hat{E}^{n+1}_{i,j} = \Delta\hat{E}^{\overline{n+1}}_{i,j} \\
\text{step 6:}\quad \hat{E}^{n+1}_{i,j} = \tfrac{1}{2}\left(\hat{E}^{n}_{i,j} + \hat{E}^{\overline{n+1}}_{i,j} + \delta\hat{E}^{n+1}_{i,j}\right)
\end{gathered} \tag{8}$$

$|\hat{A}|$ , $|\hat{B}|$ are matrices with positive eigenvalues, related to the Jacobians:

$$\hat{A} = \frac{\partial \hat{F}}{\partial \hat{E}} \ , \ \hat{B} = \frac{\partial \hat{G}}{\partial \hat{E}} \tag{9}$$

$\Delta^{+} / \Delta\xi$ and $\Delta^{+} / \Delta n$ are one-sided forward differences, $\Delta^{-} / \Delta\xi$ and $\Delta^{-} / \Delta n$ are one-sided backward differences. The Jacobians $\hat{A}$ and $\hat{B}$ are related to $A = \partial F / \partial E$ and $B = \partial G / \partial E$ , with the following equations as Lavante and Thompkins [9]:

$$\hat{A} = A\xi_x + B\xi_y \tag{10}$$

$$\hat{B} = An_x + Bn_y \tag{11}$$

$$\hat{A} = \begin{bmatrix} 0 & \xi_x & \xi_y \\ c^2\xi_x - uU & U + u\xi_x & u\xi_y \\ c^2\xi_y - vU & v\xi_x & U + v\xi_y \end{bmatrix} \tag{12}$$

$$\hat{B} = \begin{bmatrix} 0 & n_x & n_y \\ c^2 n_x - uV & V + un_x & un_y \\ c^2 n_y - vV & vn_x & V + vn_y \end{bmatrix} \tag{13}$$

Here $c^2$ = gh. The integration scheme of eqs. (7) – (8) can be much simplified by diagonalizing $\hat{A}$ and $\hat{B}$ , thus facilitating the numerical scheme convergence. Once the eigenvalues of $\hat{A}$ and $\hat{B}$ are known, it is possible to express $\hat{A}$ and $\hat{B}$ in the form as Lavante and Thompkins [9]:

$$\hat{A} = \hat{S}_{\xi}^{-1} \Lambda_A \hat{S}_{\xi} , \quad \hat{B} = \hat{S}_{n}^{-1} \Lambda_B \hat{S}_{n} \tag{14}$$

$\Lambda_A$ and $\Lambda_B$ are diagonal matrices consisting of the eigenvalues of $\hat{A}$ and $\hat{B}$ :

$$\Lambda_A = \begin{vmatrix} U & 0 & 0 \\ 0 & U + c\sqrt{\xi_x^2 + \xi_y^2} & 0 \\ 0 & 0 & U - c\sqrt{\xi_x^2 + \xi_y^2} \end{vmatrix} , \Lambda_B = \begin{vmatrix} V & 0 & 0 \\ 0 & V + c\sqrt{n_x^2 + n_y^2} & 0 \\ 0 & 0 & V - c\sqrt{n_x^2 + n_y^2} \end{vmatrix} \tag{15}$$

The matrices $\hat{S}_{\xi}$ and $\hat{S}_{\eta}$ are given as the product of two matrices:

$$\hat{S}_{\xi} = L_{\xi}^{-1} M^{-1} , \hat{S}_{n} = L_{n}^{-1} M^{-1} \tag{16}$$

For each, the right matrix represents a transformation from conservative to non-conservative form variables and the left matrix transforms from non-conservative to characteristic form. The M matrix is calculated as:

$$M = \frac{\partial E}{\partial H} \tag{17}$$

with $E = [h \quad hu \quad hv]^T$ and $H = [h \quad u \quad v]^T$ . The $L_\xi$ matrix with unknown values ($x_1$, $x_2$, $x_3$) can be found by solving the systems:

$$[x_1 \quad x_2 \quad x_3] \left[\tilde{A}\right] = \lambda_i \, [x_1 \quad x_2 \quad x_3] \tag{18}$$

$\lambda_i$ (i=1,3) are the eigenvalues of $\Lambda_A$ , $\lambda_1 = U$ , $\lambda_2 = U + C\sqrt{\xi_x^2 + \xi_y^2}$ and $\lambda_3 = U - C\sqrt{\xi_x^2 + \xi_y^2}$ .

The $L_\eta$ matrix with unknown values ($y_1$, $y_2$, $y_3$) can be found by solving the systems:

$$[y_1 \quad y_2 \quad y_3] \left[\tilde{B}\right] = \lambda_j \, [y_1 \quad y_2 \quad y_3] \tag{19}$$

$\lambda_j$ (j=1,3) are the eigenvalues of $\Lambda_B$ , $\lambda_1 = V$ , $\lambda_2 = V + C\sqrt{n_x^2 + n_y^2}$ and $\lambda_3 = V - C\sqrt{n_x^2 + n_y^2}$ .

The matrices $\tilde{A}$ and $\tilde{B}$ are the non-conservative form of $\hat{A}$ and $\hat{B}$ and both of them have the same eigenvalues and are calculated as:

$$\tilde{A} = M^{-1}\hat{A}\, M , \quad \tilde{B} = M^{-1}\hat{B}\, M \tag{20}$$

The matrices $\hat{S}_{\xi}$ and $\hat{S}_{\eta}$ are calculated as:

$$\hat{S}_{\xi}=\begin{bmatrix}0 & -\xi_y a_1/\xi_x & a_1\\ a_2 & h\xi_x a_2/(c\theta i) & h\xi_y a_2/(c\theta i)\\ a_3 & -h\xi_x a_3/(c\theta i) & -h\xi_y a_3/(c\theta i)\end{bmatrix}\begin{bmatrix}1 & 0 & 0\\ -u/h & 1/h & 0\\ -v/h & 0 & 1/h\end{bmatrix}=L_{\xi}^{-1}M^{-1}$$
$$\hat{S}_{n}=\begin{bmatrix}0 & b_1 & -n_x b_1/n_y\\ b_2 & hn_x b_2/(c\theta i) & hn_y b_2/(c\theta i)\\ b_3 & -hn_x b_3/(c\theta i) & -hn_y b_3/(c\theta i)\end{bmatrix}\begin{bmatrix}1 & 0 & 0\\ -u/h & 1/h & 0\\ -v/h & 0 & 1/h\end{bmatrix}=L_{n}^{-1}M^{-1} \quad (21)$$

$a_1$, $a_2$, $a_3$ and $b_1$, $b_2$, $b_3$ are arbitrary constants and $\theta_i=\sqrt{\xi_x^2+\xi_y^2}$ or $\theta_i=\sqrt{n_x^2+n_y^2}$ . Now the integration scheme of eq. 7 (predictor) can be carried out in the following steps:

$\Delta\hat{E}_{i,j}^{n}$ at every point inside the calculation domain is given as:

$$\Delta\hat{E}_{i,j}^{n}=-\Delta t\left(\frac{\Delta^{+}\hat{F}_{i,j}^{n}}{\Delta\xi}+\frac{\Delta^{+}\hat{G}_{i,j}^{n}}{\Delta n}-\hat{Q}^{n}\right) \quad (22)$$

The following form is solved:

$$\left(I-\Delta t\frac{\Delta^{+}\left|\hat{A}\right|^{n}}{\Delta\xi}\right)\left(I-\Delta t\frac{\Delta^{+}\left|\hat{B}\right|^{n}}{\Delta\eta}\right)\delta\hat{E}_{i,j}^{\overline{n+1}}=\Delta\hat{E}_{i,j}^{n} \quad \text{for} \quad \delta\hat{E}_{i,j}^{\overline{n+1}} \quad (23)$$

This is done in two steps by denoting:

$$\left(I-\Delta t\frac{\Delta^{+}\left|\hat{B}\right|^{n}}{\Delta n}\right)\delta\hat{E}_{i,j}^{\overline{n+1}}=\delta\hat{E}_{i,j}^{*} \quad (24)$$

resulting in two vector equations:

$$\left(I-\Delta t\frac{\Delta^{+}\left|\hat{A}\right|^{n}}{\Delta\xi}\right)\delta\hat{E}_{i,j}^{*}=\Delta\hat{E}_{i,j}^{n} \qquad (\delta\hat{E}_{i,j}^{*}\text{ operates on the }\Delta t\frac{\Delta^{+}\left|\hat{A}\right|^{n}}{\Delta\xi}) \quad (25)$$

$$\left(I-\Delta t\frac{\Delta^{+}\left|\hat{B}\right|^{n}}{\Delta n}\right)\delta\hat{E}_{i,j}^{\overline{n+1}}=\delta\hat{E}_{i,j}^{*} \quad (26)$$

A closer look at eq. (25) reveals that it is an upper bidiagonal equation that can be solved by sweeping in ξ direction, for a constant *n*. After simple manipulation leads to:

$$\left(I+\Delta t\hat{S}_{\xi_{i,j}}^{-1}\Lambda_{A_{i,j}}\hat{S}_{\xi_{i,j}}\right)\delta\hat{E}_{i,j}^{*}=\Delta\hat{E}_{i,j}^{n}+\Delta t\left|\hat{A}\right|_{i+1,j}^{\eta}\delta\hat{E}_{i+1,j}^{*} \quad (27)$$

Denoting $w=\Delta\hat{E}_{i,j}^{n}+\Delta t\left|\hat{A}\right|_{i+1,j}^{\eta}\delta\hat{E}_{i+1,j}^{*}$ after some matrix multiplication:

$$\hat{S}_{\xi_{i,j}}^{-1}\left(I+\Delta t\Lambda_{A_{i,j}}\right)^{-1}\hat{S}_{\xi_{i,j}}w \quad (28)$$

Equation (28) can be very easily solved since $\hat{S}_{\xi}^{-1}$ and $\hat{S}_{\xi}$ are known, eq. (21) and the inversion of the diagonal matrix $(I+\Delta t\Lambda_A)^{-1}$ is trivial. Step b) can be carried out in the same manner since $\delta\hat{E}_{i,j}^{*}$ is now known.

The corrector step, eq. (8), is analogous to the predictor step. The equation can be solved by sweeping in n direction, for a constant ξ. The major problem in the scheme described above is finding the proper boundary values of the expression $\Delta t\left|\hat{B}\right|_{i,j}\delta\hat{E}_{i,j}$ for i = IM (outlet), i = 1 (inlet) and j = JM (upper wall) and j = 1 (lower wall) because these are not know at the time when the sweep starts.

### 3.3 Calculation procedure

A more analytical presentation of the numerical method and the procedure used for solving the block bi-diagonal equation for the ξ–coordinate direction is given. The calculation procedure begins with the vectors $\Delta\hat{E}_{i,j}^{n}$ guessed for all i, j. Similarly, $\left|\hat{A}\right|\delta\hat{E}_{IM,j}^{*}$ is supposed at IM. Starting from the outlet, the calculation steps are:

1. $w=\Delta\hat{E}_{i,j}^{*}+\Delta t\left|\hat{A}\right|_{i+1,j}^{n}\delta\hat{E}_{i+1,j}^{*}$
2. $X=\hat{S}_{\xi}w$
3. Calculation of $\Lambda_A$ ,

4. $Y = \left(I + \frac{\Delta t}{\Delta \xi}\Lambda_A\right)^{-1} X$
5. $\delta \hat{E}^*_{i,j} = \hat{S}_\xi^{-1} Y$
6. $Z = \Lambda_A Y$
7. $\left|\hat{A}\right| \delta \hat{E}^*_{i,j} = \hat{S}_\xi^{-1} Z$

The matrix of inversion of step 4 is trivial because the matrix is diagonal, the solution at grid point i, j is obtained at step 5 and the flux to be used in the calculation at grid point i-1, j is obtained at step 7.

### 3.4 Boundary Conditions

All the elements $\delta \hat{E}^{predictor}_{IM,J}$ and $\delta \hat{E}^{corrector}_{1,J}$ , respectively, are set equal to zero. Along the solid walls, for the predictor step, $\delta \hat{E}^{predictor}_{i,JM+1} = \Delta t \left|\hat{B}\right|^{corrector}_{i,JM} \delta E^{corrector}_{i,JM}$ , while for the corrector step, $\delta \hat{E}^{corrector}_{i,0} = \Delta t \left|\hat{B}\right|^{predictor}_{i,1} \delta \hat{E}^{predictor}_{i,1}$ .

For supercritical case, at the inlet, the u velocity, the water depth h and the v velocity are all set at the required values, while at the outlet, all variables are extrapolated from the interior points. For subcritical case at the outlet, the water depth h is fixed and all inlet variables h, u and v are extrapolated from the interior points. To close the problem the conditions of no mass flow perpendicular to a solid wall is applied. This is achieved by requiring the V velocity components along the walls to be zero. Various convergence criteria were applied to satisfy the appropriate implicit scheme solution. Convergence criteria state that, a) the maximum velocity (or velocities) magnitude error, from iteration to iteration, within the flow field as well as b) the mass flow difference between inlet and outlet regions, to be less than $<10^{-8}$.

### 3.5 Courant-Friedrichs-Levy Condition

The above described numerical scheme is a time-marching method in which Δt must be satisfied for a solution to be achieved. For every point i, j of the computational domain the Δt time step is calculated:

$$\Delta T_1 = FT\left(\frac{1}{2}\frac{\Delta x}{(|u|+c)}\right) \quad \text{and} \quad \Delta T_2 = FT\left(\frac{1}{2}\frac{\Delta y}{(|v|+c)}\right) \tag{29}$$

$$\Delta t = \min(\Delta T_1, \Delta T_2) \tag{30}$$

and $c = \sqrt{gh}$ is the celerity. For typical supercritical applications, Rouse et al. [22], channel expansions at Fr equal to 2.0 and 4.0, the FT coefficient takes values between 1.0 and 2.0.

## 4. Explicit Finite-Volume Numerical Method

A previously developed finite-volume, explicit numerical scheme, applied for the determination of free-surface and other hydrodynamic variations in different open channel geometries, is used in order to compare current numerical results. Navier-Stokes equations were solved in an integral form and have been applied to a series of finite-volumes with adjacent volumes sharing a common face Farsirotou [21] and Farsirotou et al [2]. At the end of each time step Δt the net flux into each elemental volume is zero, so that overall water mass flow is conserved and the changes in momentum are equal to the forces imposed by system's boundaries. The two-dimensional flow eq. (1) may be written down as conservation equations for a control volume ΔV of unit height and for a time step Δt as:

$$-\Delta h = \left[\Delta(hu)\Delta y + \Delta(hv)\Delta x\right]\frac{\Delta t}{\Delta x \Delta y} \tag{31}$$

$$\begin{aligned}-\Delta(hu) = {} & \left[\Delta\left(gh^2/2 + hu^2\right)\Delta y + \Delta(huv)\Delta x\right]\frac{\Delta t}{\Delta x \Delta y} + gh\left(S_{ox} + S_{fx}\right)\Delta t - \\ & \left\{\Delta\left[2.0\nu_t\,\Delta(hu)\right]\Delta y\,\frac{\Delta x}{\Delta x \Delta x} + \Delta\left[\nu_t \Delta(hu)\Delta x + \nu_t \Delta(hv)\Delta y\right]\frac{\Delta x}{\Delta x \Delta y}\right\}\frac{\Delta t}{\Delta x \Delta y}\end{aligned} \tag{32}$$

$$\begin{aligned}-\Delta(hv) = {} & \left[\Delta\left(gh^2/2 + hv^2\right)\Delta x + \Delta(huv)\Delta y\right]\frac{\Delta t}{\Delta x \Delta y} + gh\left(S_{oy} + S_{fy}\right)\Delta t - \\ & \left\{\Delta\left[2.0\nu_t\,\Delta(hv)\right]\Delta x\,\frac{\Delta y}{\Delta y \Delta y} + \Delta\left[\nu_t \Delta(hu)\Delta x + \nu_t \Delta(hv)\Delta y\right]\frac{\Delta y}{\Delta x \Delta y}\right\}\frac{\Delta t}{\Delta x \Delta y}\end{aligned} \tag{33}$$

Figure 2 shows the notation used for mass flux balancing across a finite-volume of the flow and a flowchart of the explicit finite-volume numerical technique. Similar notation is adopted for the balancing of the x-momentum and y-momentum. Thus, for the water mass flux, an XFLUX at a point i,j is defined as:

$$(XFLUX)_{i,j} = \left[\frac{(hu)_{i+1,j} + (hu)_{i,j}}{2}\right]\Delta y \tag{34}$$

and the YFLUX, at the same point i,j is defined as:

$$(YFLUX)_{i,j} = \left[\frac{(hv)_{i,j-1}+(hv)_{i,j}}{2}\right]\Delta x - \left[\frac{(hu)_{i,j-1}+(hu)_{i,j}}{2}\right]\Delta y_B \tag{35}$$

The second term of the above equation comes from the balancing of the mass fluxes into the ABE flow region, Fig. 2. The $\Delta y_B$ term is also defined in Fig. 2. The terms $\Delta(hu)$ and $\Delta(hv)$ of (31) are defined as:

$$\Delta(hu) = (XFLUX)_{i,j} - (XFLUX)_{i,j-1} \tag{36}$$

$$\Delta(hv) = (YFLUX)_{i+1,j} - (YFLUX)_{i,j} \tag{37}$$

Similar differences are applied to all $\Delta$ terms, of Eqs. (32) and (33). Thus, the water depth difference in each finite-volume is given by:

$$\Delta h_{i,j} = -\left[(XFLUX)_{i,j} - (XFLUX)_{i,j-1} + (YFLUX)_{i+1,j} - (YFLUX)_{i,j}\right]\frac{\Delta t}{\Delta x \Delta y} \tag{38}$$

For the x-momentum flux balance, the corresponding $(XFLUX)_{i,j}$ and $(YFLUX)_{i,j}$ are defined as:

$$(XFLUX)_{i,j} = \left[\frac{\left(\frac{gh^2}{2}+hu^2\right)_{i,j} + \left(\frac{gh^2}{2}+hu^2\right)_{i+1,j}}{2}\right]\Delta y - 2.0\nu_t\left[\frac{\Delta(hu)_{i,j}+\Delta(hu)_{i+1,j}}{2\Delta x}\right]\Delta y \tag{39}$$

$$\begin{aligned}(YFLUX)_{i,j} = &\left[\frac{(huv)_{i,j-1}+(huv)_{i,j}}{2}\right]\Delta x - \left[\frac{\left(\frac{gh^2}{2}+hu^2\right)_{i,j} + \left(\frac{gh^2}{2}+hu^2\right)_{i,j-1}}{2}\right]\Delta y_B \\ &-\nu_t\left[\frac{\Delta(hu)_{i,j}+\Delta(hu)_{i,j-1}}{2\Delta y} + \frac{\Delta(hv)_{i,j}+\Delta(hv)_{i,j-1}}{2\Delta x}\right]\Delta x + 2.0\nu_t\left[\frac{\Delta(hu)_{i,j}+\Delta(hu)_{i,j-1}}{2\Delta x}\right]\Delta y_B\end{aligned} \tag{40}$$

Thus, the difference $\Delta(hu)$ in each finite volume is given as:

$$\Delta(hu)_{i,j} = -\left[(XFLUX)_{i,j} - (XFLUX)_{i,j-1} + (YFLUX)_{i+1,j} - (YFLUX)_{i,j}\right]\frac{\Delta t}{\Delta x \Delta y} - gh(S_{ox}+S_{fx})\Delta t \tag{41}$$

Similarly, for the y-momentum flux balance, the corresponding $(XFLUX)_{i,j}$ , $(YFLUX)_{i,j}$ and the difference $\Delta(hv)$ for each finite volume are defined. Backward differencing is used for the $\Delta/\Delta x$ estimation, while forward differencing is used for the $\Delta/\Delta y$ estimation and analytical presentation of the explicit method solution is given by Farsirotou [21].

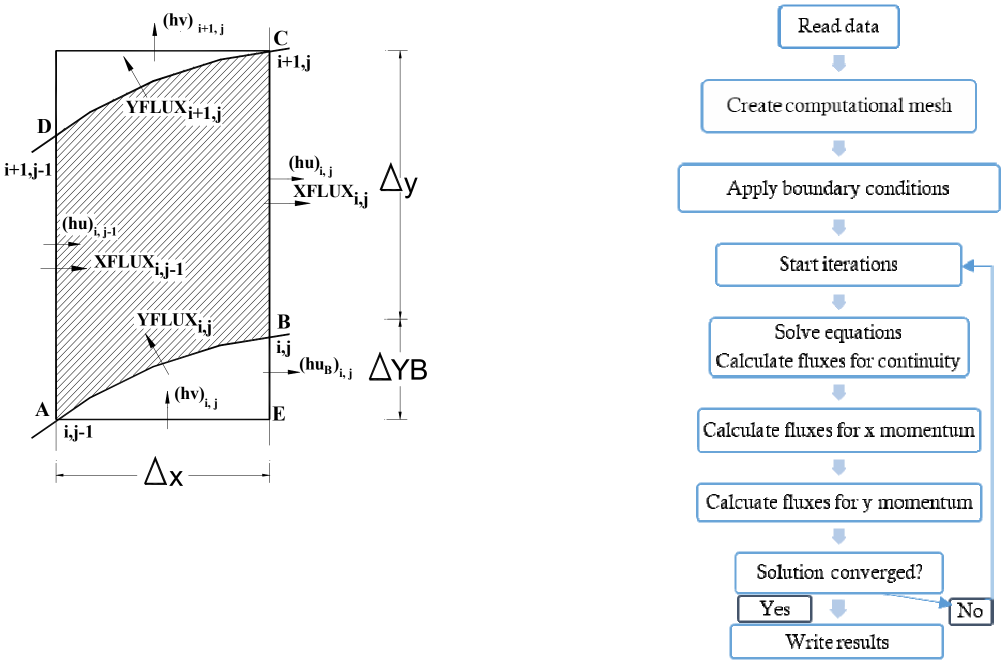


(a) (b)

**Fig. 2.** a) Notation for the mass flux across a finite-volume and b) flowchart for the explicit method.

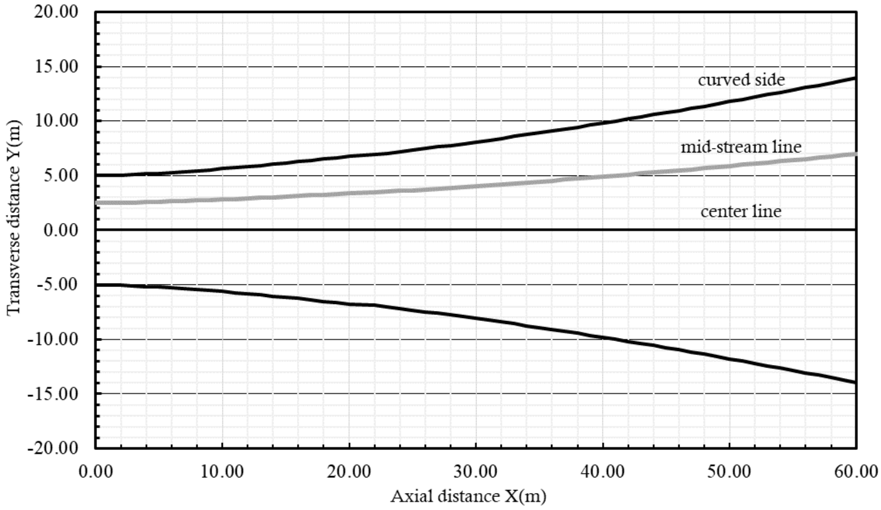


**Fig. 3.** Flume geometry with stream lines.

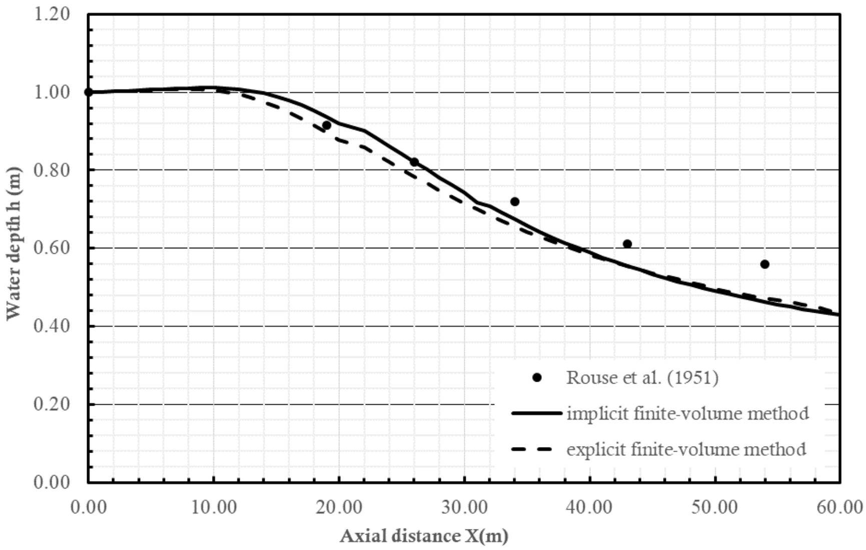


**Fig. 4.** Water depth comparison between numerical simulation predictions and measurements for the Rouse et al. [22] channel along the center line at Fr=4.

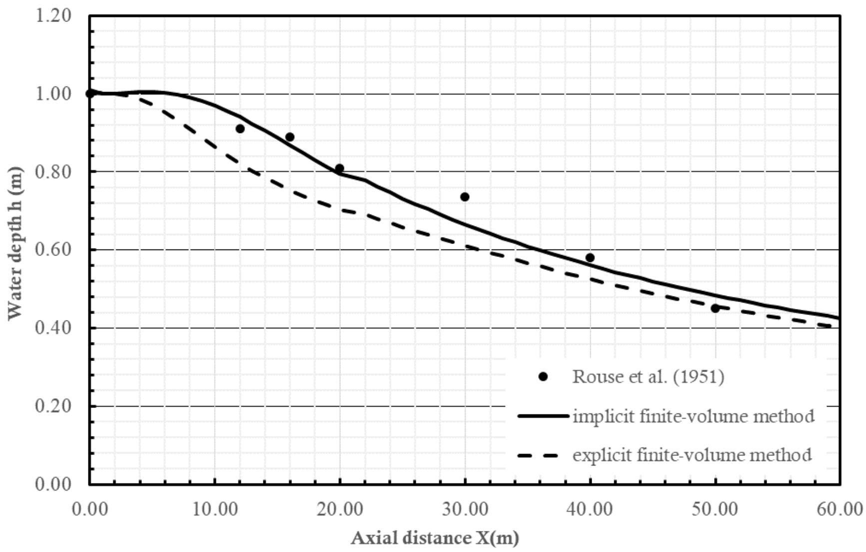


**Fig. 5.** Water depth comparison between numerical simulation predictions and measurements for the Rouse et al. [22] channel along the mid-stream line at Fr=4.

## 5. Computational Results and Discussion

It is well known that implicit solvers speed up the solution convergence. The time-step (CFL criterion) of the implicit numerical schemes is relatively large compared to the explicit one. Thus, the solution convergence requires smaller iteration numbers. Most of the implicit techniques require tri-diagonal or penta-diagonal system of equations solution resulting into considerable central processing unit time consumption.

An implicit numerical technique, which was initially introduced by MacCormack [10] for compressible flows, was developed and subsequently programmed and applied for free-surface flows. The expression of Navier-Stokes equations in terms of semi-linearization and diagonalization matrices makes possible the application of implicit bi-diagonal numerical schemes. This procedure greatly facilitates the solution convergence since only two unknown elements are solved in each row of the resulting linear system of equations. The scheme was unconditionally stable and very efficient in that no block or scalar tri-diagonal inversions were required for solution. It belongs to the multi-step numerical approach with predictor and corrector steps. The widely accepted pseudo-compressibility technique was currently applied to solve shear flow hydrodynamic problems incorporating bi-diagonal implicit scheme.

A question arises as how fast the implicit bi-diagonal scheme solution convergence was compared to an explicit formulation technique. The obvious task was to evaluate their numerical performance in terms of accuracy, stability and fast convergence. The solution convergence performance ability configuration for either numerical methods is better elucidated using smooth geometry since errors induced from local geometry errors are minimal. This is particularly true for multi-dimensional geometry flows.

Numerous numerical experimentation tests were currently performed to establish the speed of the solution convergence. All comparisons between explicit and implicit schemes were performed under optimum convergence factors of either methods. For the explicit technique, the required CPU time per iteration was small compared to the implicit one. However, the required total iteration number is considerably high. Thus, the total CPU time for the implicit formation is substantially small. Currently developed algorithms are relatively simple although a lot of programming effort is required for the implicit technique formulation. Programming of either methods was enforced via Fortran language. For the implicit method, numerous subroutines were incorporated to facilitate the matrix calculation complexity. The semi-linearization matrices as well as the matrix diagonalizations are somehow difficult to handle. The expense in programming effort is justified in terms of convergence acceleration. The bi-diagonal, implicit formation, finite-volume method and the Mac-Cormack predictor-corrector method application resulted into robust and fast numerical methodology.

The validity of the proposed computational techniques was tested for steady, supercritical, free-surface flow conditions. It may be mentioned that for all test cases there were experimental data available for comparison. Computed results from both numerical methodologies were satisfactorily compared with experimental measurements. The convergence performance was possible to be carried out by direct comparisons.

### 5.1 Channel Expansion at Fr= 4.0

The channel geometry shown in Fig. 3. was used to test the accuracy and convergence solution of the depth-averaged implicit numerical method, at high entrance Froude numbers, by comparing it with the explicit, finite-volume, numerical technique of Farsirotou et al. [2] as well as with experimental measurements of Rouse et al. [22]. An approach Froude number equal to $Fr_1$=4.0 at the inflow boundary has been chosen in order to verify both numerical models. The actual channel geometry is given by the formula:

$$\frac{y}{b_1}=\frac{1}{2}\left(\frac{x}{4.0b_1}\right)^{3/2}+\frac{1}{2} \tag{42}$$

$b_1$ is the half entrance channel width. At the entrance the channel width is 10.0 m and the channel length 60.0 m. The grid point density was kept high enough so as the flow quantities to be properly resolved. For the same hydraulic boundary conditions numerical results were obtained using two different computational meshes, a coarse mesh 61x19 (axial x tangential) and a fine mesh 61x29 in order to perform a mesh sensitivity analysis for the explicit and the implicit finite-volume model. Relative errors of the calculated water depths according to the experimental measurements of water depth are calculated as:

$$relative\ error\ [\%]=\left(\frac{h_{model}-h_{experimental}}{h_{experimental}}\right)\times 100 \tag{43}$$

$h_{model}$ is each water depth numerical simulation prediction at the same point of the experimental measurements and $h_{experimental}$ is each experimental water depth value. For the coarse mesh the relative errors of the calculated water depths are between 0.1% and 0.8% while for the fine mesh between 0.04% and 0.6%. Numerical results based on the 61x29 mesh size are presented, for both numerical models, as there is smaller deviation compared with available experimental measurements. As the flow is supercritical, boundary conditions must be applied only at the upstream boundary channel. The upstream boundary condition used is the inlet water depth equal to 1.0 m and the axial velocity magnitude equal to 12.52 m/s with zero value transverse velocity component. Bottom slopes of $S_{ox}$ = 0.0 ‰ and $S_{oy}$ = 0.0 ‰ and Manning flow friction coefficient n = 0.012 were also used for the simulation. Comparisons between the two numerical predictions (explicit and implicit) and measurements for the water depth variation in the above channel are shown in Figs 4, 5 and 6 for three different stream lines presented in Fig.3, the center line (axis of symmetry), the mid-stream line (equally distanced between curved side and center line) and the curved side, respectively. The water surface within the expansion fits very well between measurements and simulation. Figure 7 shows the convergence histories of the two numerical techniques for the under consideration test case. Calculations for the implicit technique stopped after 350 iterations, when the average error in the axial velocity change between two successive iterations dropped below $1.0\text{x}10^{-7}$. The explicit numerical method, converged after 5000 iterations. Thus, the implicit technique is substantially faster to the explicit one in terms of required iterations for achieving convergence.

### 5.2 Channel Expansion at Fr = 2.0

An approach Froude number equal to $Fr_1$=2.0 at the inflow boundary has been used as second test case for the validation of the numerical model. The actual channel geometry is given by the formula:

$$\frac{y}{b_1}=\frac{1}{2}\left(\frac{x}{2.0b_1}\right)^{3/2}+\frac{1}{2} \tag{44}$$

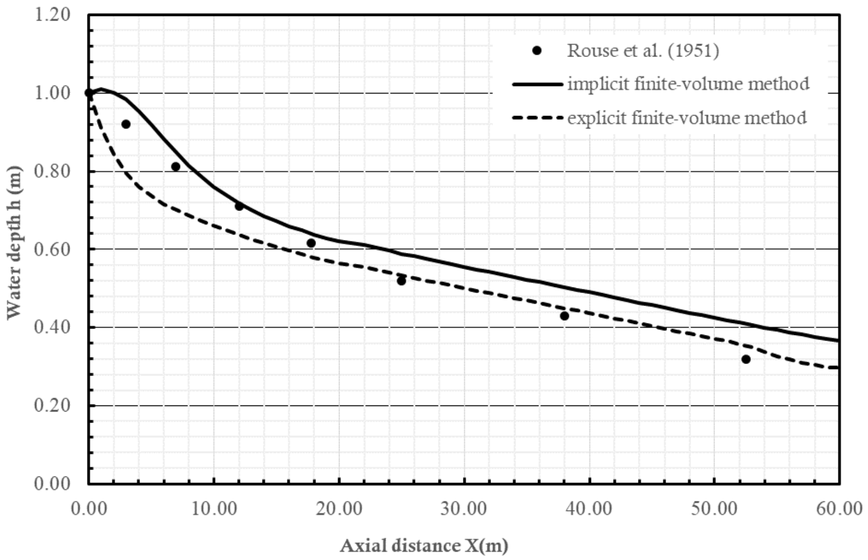


**Fig. 6.** Water depth comparison between numerical simulation predictions and measurements for the Rouse et al. [22] channel along the curved line at Fr=4.

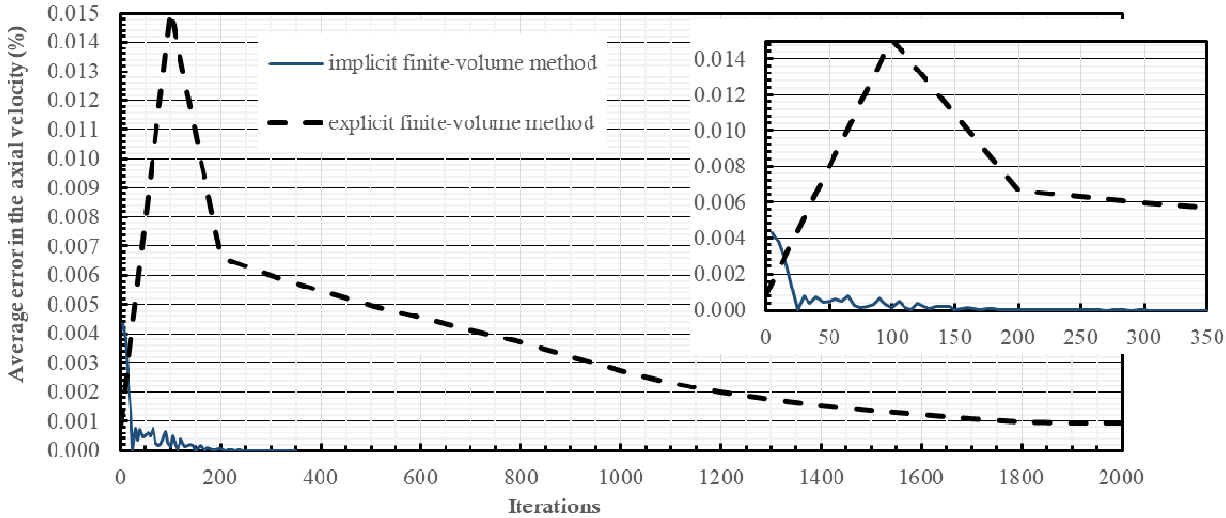


**Fig. 7.** Convergence history comparisons between method predictions for the Rouse et al. [22] expansion channel at Fr=4. Embedded scheme shows the convergence history of the two methods up to 350 iterations.

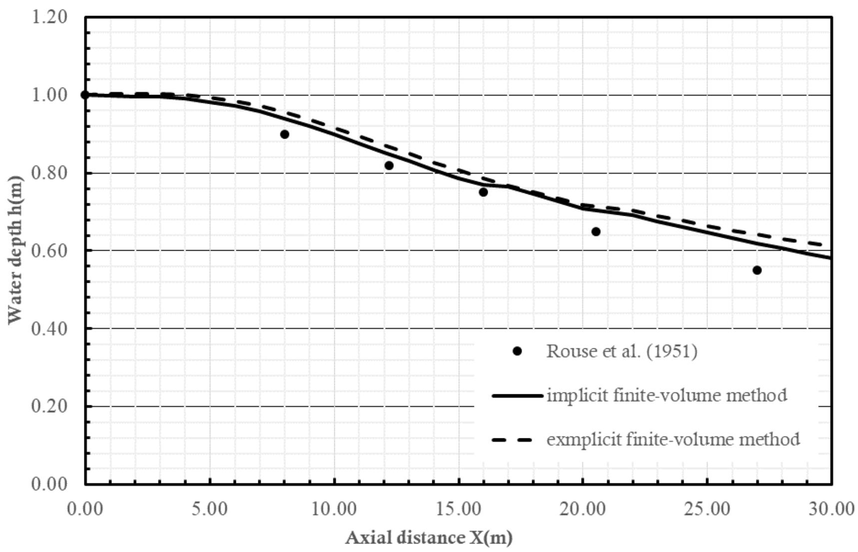


**Fig. 8.** Water depth comparison between numerical simulation predictions and measurements for the Rouse et al. [22] channel along the center line at Fr=2.

**Table 1.** Maximum relative errors of the numerical results.

| a/a | Numerical simulation test case | Maximum relative error (%) | |
|---|---|---|---|
| | | Coarse mesh | Fine mesh |
| 1 | Explicit model, Fr=4.0 | 0.80 | 0.60 |
| 2 | Implicit model, Fr=4.0 | 0.70 | 0.56 |
| 3 | Explicit model, Fr=2.0 | 0.80 | 0.65 |
| 4 | Implicit model, Fr=2.0 | 0.76 | 0.60 |

$b_1$ is the half entrance width. At the entrance the channel width is 10.0 m and the channel length is 30.0 m. The upstream boundary condition used is the inlet water depth equal to 1.0 m and the axial velocity magnitude equal to 6,264 m/s with zero value transverse velocity component. Computational mesh was also examined using a coarse mesh 31x15 (axial x tangential) and a fine mesh 31x25. The fine mesh was utilized, for both numerical techniques, according to the results of maximum relative errors computed from eq. (43), given in Table 1, for each numerical simulation test case. Comparisons between numerical predictions and measurements for the water depth variation are shown in Figs. 8, 9 and 10 for the centerline, mid-stream line and curved side, respectively. Agreement with measurements seems to be satisfactory. Figure 11 shows the convergence histories of the two methods (implicit and explicit) for the under consideration test case. Calculations for the implicit method stopped after 170 iterations, when the average error in the axial velocity change between successive iterations dropped below $1.0\text{x}10^{-7}$. The explicit numerical method, converged after 5000 iterations (very slow convergence indeed).

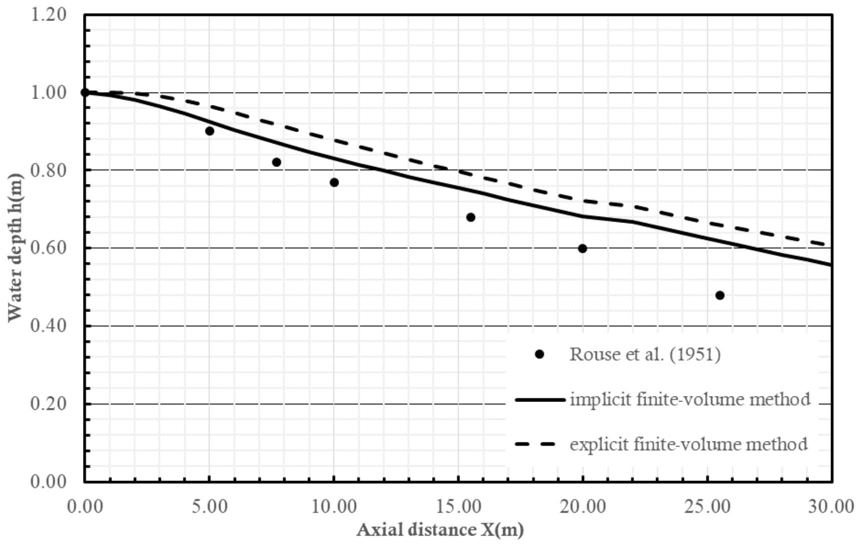


**Fig. 9.** Water depth comparison between numerical simulation predictions and measurements for the Rouse et al. [22] channel along the mid-stream line at Fr=2.

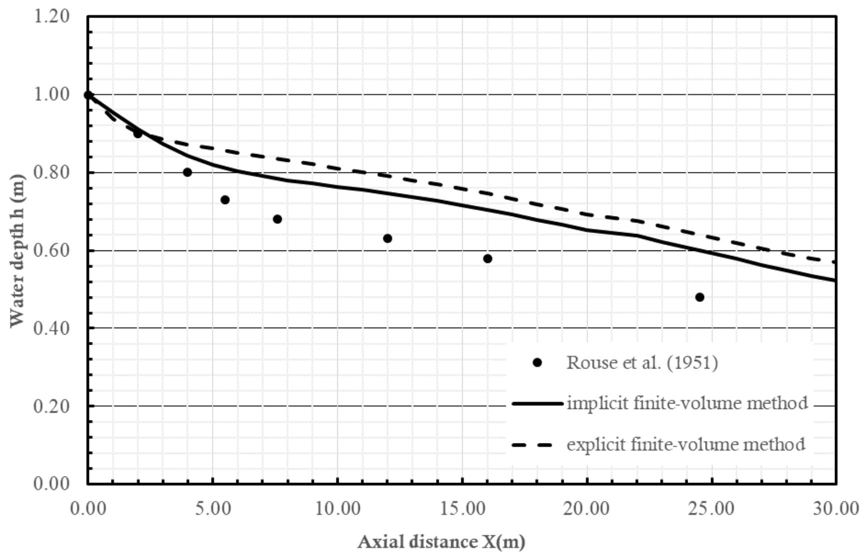


**Fig. 10.** Water depth comparison between numerical simulation predictions and measurements for the Rouse et al. [22] channel along the curved line at Fr=2.

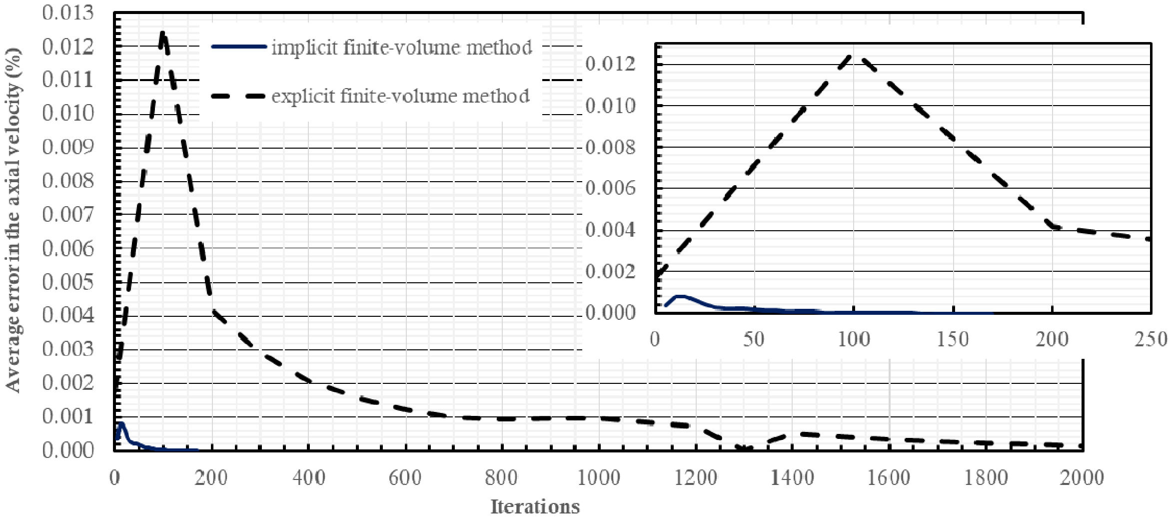


**Fig. 11.** Convergence history comparisons between method predictions for the Rouse et al. [22] expansion channel at Fr=2. Embedded scheme shows the convergence history of the two methods up to 250 iterations.

## 6. Conclusion

Computational results of water surface variation and convergence performance between two different finite-volume numerical schemes were presented. The objective of the current research is to investigate the speed of the solution convergence of an implicit and an explicit finite-volume numerical scheme, for incompressible, viscous, depth-averaged free-surface, steady flows. An implicit, bi-diagonal, numerical scheme, based on MacCormack's predictor- corrector technique and an explicit, integral numerical method were used. Numerical results of water depth variation were satisfactorily compared with available measurements for both numerical techniques. The implicit bi-diagonal technique yields fast convergence compared to the explicit one at the expense of programming effort. Iterations required to achieve convergence solution error of less than $10^{-5}$ can be reduced down to 90.0 % in comparison to analogous flows with using explicit numerical technique. Near future extensions will include the development of the implicit method under unsteady flow conditions in conjunction with bed morphology variation, which was adequately performed with the explicit method, in order to improve the speed of the solution convergence in more complicated hydrodynamic and sediment transport conditions.

## Author Contributions

The manuscript was written through the contribution of all authors. All authors discussed the results, reviewed and approved the final version of the manuscript.

## Conflict of Interest

The authors declared no potential conflicts of interest with respect to the research, authorship and publication of this article.


## Funding

The authors received no financial support for the research, authorship and publication of this article.


## Nomenclature

| | | | |
|---|---|---|---|
| $h$ | Water depth [m] | $g$ | Gravity acceleration [m/s$^2$] |
| $u, v$ | Average velocity components [m/s] | $n$ | Manning's flow friction coefficient |
| $S_{ox}$ , $S_{oy}$ | Bottom slopes [m/m] | $t$ | Time [s] |
| $S_{fx}$ , $S_{fy}$ | Flow friction slopes [m/m] | $x, y$ | Cartesian coordinate positions [m] |
| $z$ | Bed level [m] | $\xi, n$ | Local coordinates [m] |
| $Fr$ | Froude number | $J$ | Transformation matrix |
| $v_t$ | Kinematic viscosity [m$^2$/s] | | |

## References


[1] Bradford, S.F. and Sanders, B.F., Finite-volume model for shallow-water flooding of arbitrary topography. *Journal of Hydraulic Engineering*, 128(3), 2002, 289–298.

[2] Farsirotou, E.D., Dermissis, V.D. and Soulis, J.V., A numerical method for two-dimensional bed morphology calculations. *Journal of Computational Fluid Dynamics*, 16(3), 2002, 187-200.

[3] Fernandez, J.P., Morales, H.M. and Garcia, N.P., Implicit finite volume simulation of 2D shallow water flows in flexible meshes. *Journal of Computer Methods in Applied Mechanics and Engineering,* 328(1), 2018, 1-25.

[4] Fu, L. and Jin, Y.C., A mesh-free method boundary condition technique in open channel flow simulation, *ASCE Journal of Hydraulic Engineering,* 51(2), 2013, 174-185.

[5] Gaffar, S.A., Reddy, P.R., Prasad, V.R., Rao, A.S. and Khan, M.H., Viscoelastic micropolar convection flows from an inclined plane with nonlinear temperature: A numerical study. *Journal of Applied Research in Water and Wastewater,* 6(2), 2020, 183-199.

[6] Gholami, A., Bonakdari, H. and Akhtari, A.A., Developing finite volume method (FVM) in numerical simulation of flow pattern in 60° open channel bend. *Journal of Applied Research in Water and Wastewater,* 3(1), 2016, 193-200.
[7] Kassem, A.A. and Chaudhry, M.H., Comparison of coupled and semicoupled numerical models for alluvial channels. *ASCE Journal of Hydraulic Engineering,* 124(8), 1998, 794–802.
[8] Klonidis, A.J. and Soulis, J.V., An implicit scheme for steady two - dimensional free-surface flow calculation. *Journal of Hydraulic Research*, 39(4), 2001, 393-402.
[9] Lavante, V.E. and Thompkins, W., An Implicit, Bidiagonal Numerical Method for Solving the Navier - Stokes Equations. *AIAA Journal*, 21(6), 1982, 828-833.
[10] MacCormack, R.N., A Numerical Method for Solving the Equations of Compressible Viscous Flow. *AIAA Journal,* 20(9), 1982, 1275 -1281.
[11] Menni, Y., Azzi, A., Chamkha, A.J. and Harmand, S., Analysis of Fluid Dynamics and Heat Transfer in a Rectangular Duct with Staggered Baffles. *Journal of Applied and Computational Mechanics,* 5(2), 2019, 231-248.
[12] Molls, T.R., Chaudhry, M.H. and Khan, K.W., Numerical simulation of two-dimensional flow near a spur-dike. *Advances in Water Resources*, 18(4), 1995, 227-236.
[13] Molls, T.R. and Chaudhry, M.H., Depth-Averaged Open-Channel Flow Model. *Journal of Hydraulic Engineering,* 121(6), 1995, 453-465.
[14] Naik, B., Khatua, K.K., Wright, N., Sleigh, A. and Singh, P., Numerical modeling of converging compound channel flow. *Journal of Hydraulic Engineering, ASCE,* 24(3), 2017, 258-297.
[15] Panagiotopoulos, A.G. and Soulis, J.V., An implicit bi-diagonal scheme for depth averaged free sur face flow equation. *Journal of Hydraulic Engineering,* 126 (6), 2000, 425-436.
[16] Periyadurai, K., Muthtamilsevan, M. and Doh, D.H., Impact on Magnetic Field on Convective Flow of a Micropolar Fluid with two Parallel Heat Sources. *Journal of Applied and Computational Mechanics,* 5(4), 2019, 652-666.
[17] Sheng, B., Lixiang, S., Jianzhong, Z., Linghang, X., Guobing, H., Minghai, H. and Suncana, K., Two-dimensional shallow water flow modeling based on an improved unstructured finite volume algorithm. *Advances in Mechanical Engineering*, 7(8), 2018, 1-13.
[18] Soulis, J.V., A numerical method for subcritical and supercritical open channel flow calculation. *International Journal for Numerical Methods in Fluids,* 13, 1991, 437-464.
[19] Sun, G., Implicit bidiagonal numerical scheme for simulation of 2D flood waves. *Advanced Materials Research*, 356-360, 2012, 2293-2296.
[20] Vagheian, M. and Talebi, S., Introduction to the slide modeling method for the efficient solution of heat conduction calculations. *Journal of Applied and Computational Mechanics*, 5(4), 2019, 680-695.
[21] Farsirotou, E.D., *Numerical and Experimental Study of Scouring in Alluvial Channels*. Ph.D. Thesis, Department of Civil Engineering, Aristotle University of Thessaloniki, Thessaloniki, Greece, 2000.
[22] Rouse, H., Bhoota, B.V. and Hsu E.Y., Design of Channel Expansions. *Trans. ASCE*, 116, 1951, 347-363.

## ORCID iD

Evangelia D. Farsirotou https://orcid.org/0000-0003-0641-8216
Alexander D. Panagiotopoulos: https://orcid.org/0000-0001-9749-2811
Johannes V. Soulis https://orcid.org/0000-0002-2640-907X



How to cite this article: Farsirotou E.D., Panagiotopoulos A.D., Soulis J.V. Explicit and Implicit Finite -Volume Methods for Depth Averaged Free-Surface Flows, *J. Appl. Comput. Mech.*, 6(SI), 2020, 1270–1282. https://doi.org/10.22055/JACM.2020.32402.2008